BIOCHEMISTRY
including biophysical chemistry & molecular biology
Article

Biochemistry **2011,** *50,* 843–853 843
DOI: 10.1021/bi1017396

The Mouse Eugenol Odorant Receptor: Structural and Functional Plasticity of a Broadly Tuned Odorant Binding Pocket

Olivia Baud,[‡] Sylvain Etter,[‡] Morena Spreafico,[§] Lorenza Bordoli,[§] Torsten Schwede,[§] Horst Vogel,*[,‡] and Horst Pick*[,‡]

[‡]*Institut des Sciences et Ingénierie Chimiques, Ecole Polytechnique Fédérale de Lausanne, CH-1015 Lausanne, Switzerland, and*
[§]*SIB Swiss Institute of Bioinformatics, Biozentrum der Universität Basel, CH-4056 Basel, Switzerland*

Received October 29, 2010; Revised Manuscript Received December 8, 2010

ABSTRACT: Molecular interactions of odorants with their olfactory receptors (ORs) are of central importance for the ability of the mammalian olfactory system to detect and discriminate a vast variety of odors with a limited set of receptors. How a particular OR binds and distinguishes different odorant molecules remains largely unknown on a structural basis. Here we investigated this question for the mouse eugenol receptor (mOR-EG). By screening a large odorant library, we discovered a wide range of chemical structures activating the receptor in heterologous mammalian cells. Potent agonists comprise (i) benzene, (ii) cyclohexane, or (iii) polycyclic structures substituted with alcohol, aldehyde, keto, ether, or esterified carboxylic groups. To detect those amino acids within the receptor that are in contact with a particular bound odorant molecule, we investigated how distinct mOR-EG point mutants were activated by the different odorant agonists found for the wild-type receptor. We identified 11 amino acids as a part of the receptor's ligand binding pocket. Molecular modeling predicted 10 of these residues in transmembrane helices TM3−TM6 and one in the extracellular loop between TM2 and TM3. These amino acids participate in odorant binding with variable importance depending on the type of odorant, revealing functional "fingerprints" of ligand−receptor interactions.

The mammalian olfactory receptor (OR)[1] superfamily has evolved the ability to recognize a seemingly infinite variety of chemical structures using a repertoire of only ~1000 different G protein-coupled receptors (*1*−*4*). ORs expressed in membranes of specialized sensory neurons of the olfactory epithelium are molecular detectors and transducers that convert the chemical odor information via an intracellular signaling cascade into electrical signals that are sent to the brain and experienced as smell when processed in the glomeruli at the olfactory bulb and decoded in the olfactory cortex (*5*, *6*). The ligand specificities of individual ORs are therefore key determinants in olfactory coding and perception of odor (*7*). However, since their discovery it has been difficult to match mammalian ORs to their primary ligands because of difficulties in expressing and detecting functionally active ORs in both heterologous and homologous systems (*8*−*11*).

The consensus view is that ORs identify and differentiate odors via combinatorial odorant receptor coding (*12*). Some of the best studied ORs seem to interact with a small subset of structurally related odorants, examples being rat OR-I7 with octanal (*13*), OR-M71 with acetophenone (*14*), mOR-EG with eugenol (*15*), and OR17−40 with helional (*16*). More recently, SR1, a mouse OR, that exhibits an unusually broad spectrum of structurally diverse odorants has been identified (*17*). Because of the lack of high-resolution OR structures, there is only little known about the protein structural determinants for recognition and discrimination of odorants (*15*, *18*−*21*).

ORs belong to class A of the large GPCR superfamily (*22*). High-resolution structures of a few receptors in this class currently available include those of bovine rhodopsin and opsin (*23*−*25*), and substantially modified versions of the human β2-adrenergic receptor (*26*), the turkey β1-adrenergic receptor (*27*), the adenosine receptor (*28*), the CXCR4 chemokine receptor (*29*), and the human dopamine D3 receptor (*30*). They all feature seven transmembrane helices, an extracellular N-terminus, and an intracellular C-terminus, and they share several conserved sequence motifs in the transmembrane domains that are important for receptor folding and transmembrane signaling (*31*). However, the overall level of sequence identity among the receptors is quite low (25%), making the search for ligand binding structures challenging (*32*). How the protein structure of an OR determines its function, which residues of an OR interact with odorants, and how that translates into differences in their ligand profiles are largely unknown. Highly variable residues are present in three of the seven transmembrane domains (TM3−5) of many ORs, indicating the region of the binding pocket for a large variety of odorants for which experimental proofs are just emerging (*15*, *33*).

Here we performed a detailed functional analysis of an odorant binding pocket focusing on the mouse eugenol olfactory receptor (mOR-EG) as a representative OR with a moderately broad but still selective odorant specificity. Katada et al. discovered that mOR-EG is activated by 22 distinct odorants centered

*To whom correspondence should be addressed. H.P.: e-mail, Horst.Pick@epfl.ch; phone, 0041-21-6933132; fax, 0041-21-6936190. H.V.: e-mail, Horst.Vogel@epfl.ch; phone, 0041-21-6933155; fax, 0041-21-6936190.

[1]Abbreviations: OR, olfactory receptor; mOR-EG, mouse eugenol olfactory receptor; WT, wild type; Rho-Myc, first 20 amino acids of rhodopsin fused with the c-Myc peptide epitope; TM, transmembrane helix; EL2, second extracellular loop; GPCR, G protein-coupled receptor; cAMP, cyclic adenosine monophosphate; cGMP, cyclic guanosine monophosphate; pCRE-SEAP, cAMP response element secreted alkaline phosphatase reporter plasmid; TBCHone, *tert*-butylcyclohexanone; EG, eugenol; MIEG, methylisoeugenol; MC, Mousse Cristal; OV, Orivone; WW, Wolfwood.

Published on Web 12/10/2010

around the chemical structure of the primary ligand eugenol (*15*). Here we report on the random screening of a large panel of 250 odorant compounds revealing 16 novel and very potent mOR-EG-specific agonists, which exhibit molecular structures significantly different from those of eugenol and its derivatives. These molecules represent a valuable set of molecular structures for probing the characteristics of the ligand binding pocket of the receptor.

In the absence of high-resolution structural data, molecular modeling combined with functional investigations of mutant proteins is a promising strategy for predicting OR structures with docked odorant molecules. A few studies have used homology modeling based on the known high-resolution protein structure of rhodopsin to predict amino acid residues in the odorant binding pocket of ORs (*15*, *20*). In this study, we chose the high-resolution structure of the β2-adrenergic receptor as a template for molecular modeling of mOR-EG (*26*). In combining computational methods for the prediction of functionally important amino acids with site-directed mutagenesis, we were able to identify five new single residues located in TM3, -5, and -6 and also the functional contribution of the second extracellular loop in ligand recognition. Taking also into account the six additional residues previously described by Katada et al. to be essential in mOR-EG for binding the primary ligand eugenol (*15*), we investigated here the functional relevance of 11 amino acids of mOR-EG for detecting and discriminating quite diverse odorant structures. We show a detailed comparison of the binding mode of four structural classes of mOR-EG-specific odorants providing insights into the localization, functionality, and three-dimensional structure of an odorant binding site of a broadly responsive OR. Our findings have implications for the understanding of olfactory coding in mammals.

MATERIALS AND METHODS

Reagents. Odorants activating mOR-EG were from Givaudan and Sigma. They were freshly dissolved in DMSO before experiments and diluted to the indicated concentrations with DMEM (Invitrogen). The cDNA of mOR-EG (*15*) was amplified from the pME18SRhoEG expression vector (S. Touhara, University of Tokyo, Tokyo, Japan) with insertion of an SpeI site at the N-terminus and subcloned into the Rho-Myc pBIISK vector. After digestion with HindII/NotI, the Rho-Myc EGOR insert was subcloned into the pCEP4 vector. mOR-EG mutants Ser113Ala, Ser113Thr, Asn207Ala, Leu212Val, Phe252Leu, Ile256Leu, and Leu259Val were kindly provided by K. Touhara and S. Katada (University of Tokyo). For all experiments, we used a, HEK 293T cell line stably expressing RTP1, RTP2, REEP1, and $G\alpha_{olf}$ (*34*).

Site-Directed Mutagenesis. Mutations were introduced by polymerase chain reaction (PCR) using a reaction mixture containing 20 ng of Rho-Myc EGOR (pCEP4 vector), 125 ng of oligonucleotide primers, 2.5 units of Pfu turbo polymerase, 5 μL of reaction buffer, and 1 μL of dNTP mix to which had been added deionized sterile water to produce a reaction volume of 50 μL (Quickchange mutagenesis kit, Stratagene, La Jolla, CA). All mutations were confirmed by sequence analysis (Microsynth, Balgach SG, Switzerland).

cAMP Reporter Gene Assay. Confluent Hana 3A cells (35000 cells per well) cultured in a 96-well plate at 37 °C (Perkin-Elmer) were transfected with 0.15 μg of the receptor cDNA and 0.15 μg of the cAMP response element secreted alkaline phosphatase reporter plasmid (pCRE-SEAP) using Lipofectamine 2000 (Invitrogen). Cells were induced 8 h after transfection with cell medium containing either the ligand or cell medium alone. Cellular responses were measured 16 h after addition of odorants. An aliquot of supernatant from each well was then mixed with an equal volume of 1 M diethanolamine bicarbonate (pH 9.8) containing 20 mM *p*-nitrophenyl phosphate and 1 mM $MgCl_2$ (Sigma). The kinetics of hydrolysis of *p*-nitrophenol phosphate by alkaline phosphatase was determined by measuring the absorbance at 410 nm using a multiwell plate reader (SpectraMax 360, Molecular Devices).

Cell-Surface Flow Cytometry. Hana 3A cells were split into a 24-well plate (TPP) with a density of 150000 cells per well (500 μL/well) and transfected with 0.8 μg of the receptor cDNA using lipofectamine. Flow cytometry analysis was performed 36 h after transfection. The cells were washed once with ice-cold PBS and then incubated for 15 min on ice with PBS containing 5% fetal bovine serum (FBS). The cells were then labeled with anti-rhodopsin 4D2 antibody (diluted 1:100 from stock) and ATTO 488 anti-mouse IgG (diluted 1:1000 from stock) and filtered through a nylon mesh to remove aggregates (BD Biosciences). Fluorescence was excited at 488 nm and monitored at 510−550 nm on a CyAn ADP high-performance flow cytometer (Beckman Coulter). Approximately 30000 events were recorded. Histograms represent the fluorescence intensity versus the number of event counts. Normalization was obtained by dividing each event count by the total number of counts.

Molecular Modeling and Ligand Docking. Homology models for the mouse eugenol receptor (mEG-OR) were built on the basis of the high-resolution crystal structure of the β2-adrenergic receptor (*26*, *35*). Multiple-sequence alignment between the mouse eugenol receptor (UniProt entry Q920P2) and several receptor orthologues was generated on the basis of the structure of the β2-adrenergic receptor and bovine rhodopsin (*23*) using 3D_COFFEE (*36*). This initial target−template alignment was further modified via incorporation of Bayesian pairwise interactions of neighboring residues (*37*), GPCR-specific fingerprints (*38*), and functional mutation studies (*15*). Coordinates of different structural models were generated using MODELER (*39*) on the basis of several alternative target−template alignments. Because of the sequence and structural variability among known GPCRs, the conformation of the second extracellular loop (Ser163−Leu198) was generated de novo with the loop modeling module of Rosetta 3.1 (*40*) (cyclic coordinate descent algorithm, 30000 conformations generated). Residue Cys180 was constrained to form a disulfide bond with Cys98 in TM3. Cys180 separates the loop into two parts (Ser163−Phe179 and Glu181−Leu198) that were modeled separately. A cluster analysis (threshold of 1.25 Å) was performed on the 1% most energetically favorable structures, and the conformation with the minimal energy was selected from the most populated cluster. The odorants were flexibly docked into each of the alternative receptor models using the Glide Induce Fit Protocol (*41*) of Schrödinger Suite 2007. Restraints on H-bonding interactions of Ser113 were used for ligands featuring a polar group, which is able to form a hydrogen bond with Ser113. Prior to docking, the receptor was checked for the correct orientation of Asn and Gln side chains, and both receptor and ligand were assigned ionization and tautomerization states. The receptor was subsequently subjected to *impref* restrained optimization based on the OPLS force field (version 2005), as implemented in the Schrödinger protein preparation wizard protocol. In particular, the *impref* restrained optimization consists of a series of minimization cycles performed on the whole modeled receptor amino acid sequence by imposing decreasing constraints on every atom but not on

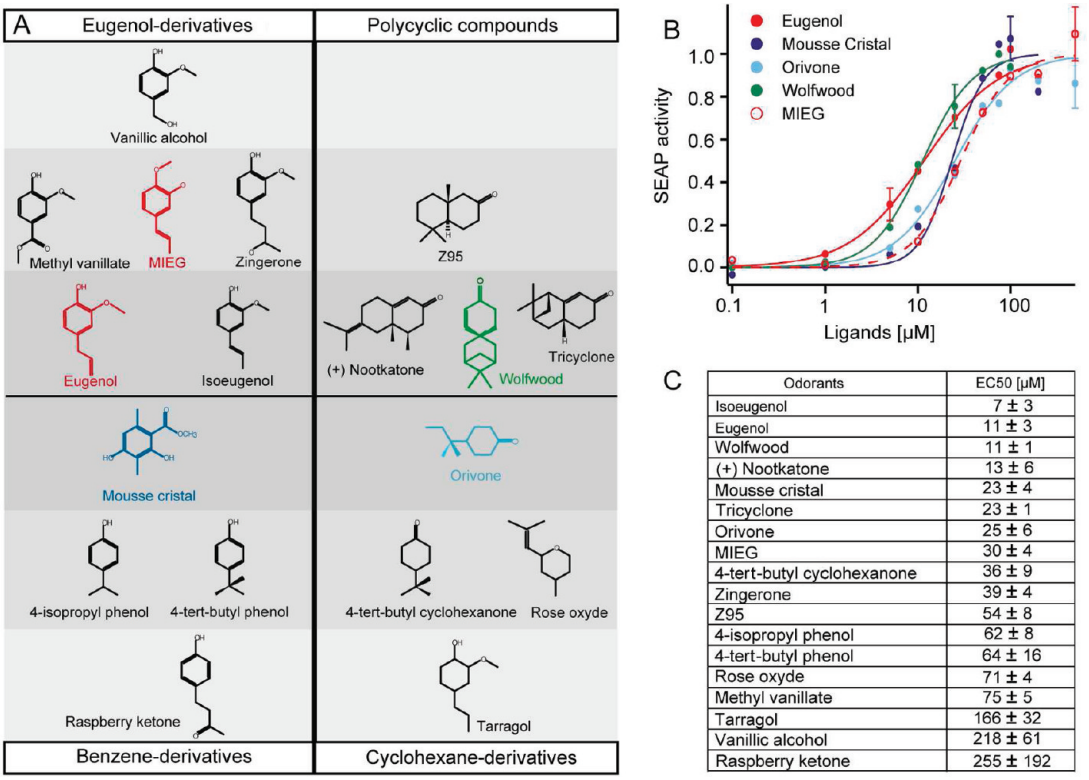

Odorants	EC50 [μM]
Isoeugenol	7 ± 3
Eugenol	11 ± 3
Wolfwood	11 ± 1
(+) Nootkatone	13 ± 6
Mousse cristal	23 ± 4
Tricyclone	23 ± 1
Orivone	25 ± 6
MIEG	30 ± 4
4-tert-butyl cyclohexanone	36 ± 9
Zingerone	39 ± 4
Z95	54 ± 8
4-isopropyl phenol	62 ± 8
4-tert-butyl phenol	64 ± 16
Rose oxyde	71 ± 4
Methyl vanillate	75 ± 5
Tarragol	166 ± 32
Vanillic alcohol	218 ± 61
Raspberry ketone	255 ± 192

FIGURE 1: Odorant agonists for mOR-EG. (A) Chemical structures of four classes of agonists (derivatives of eugenol, benzene, and cyclohexane; polycylic compounds) grouped according to EC_{50} values for activating wild-type mOR-EG: dark gray, $EC_{50} \leq 25\,\mu M$; gray, $EC_{50} = 30-100\,\mu M$; light gray, $EC_{50} > 100\,\mu M$. For colored compounds dose-response curves are shown in (B) with corresponding color code. (B) Normalized dose−response profiles of representative ligands of each structural class of odorants measured on wild-type mOR-EG. (C) Odorants ranked according to EC_{50} value for activating wild-type mOR-EG. Dose−response curves of additional mOR-EG-specific ligands are shown in Figure S1 of the Supporting Information.

hydrogens, until the maximum root-mean-square deviation of 0.30 Å from the original structure is reached. The Induced Fit Protocol includes (i) an initial step of docking using a softened potential (van der Waals radius scaling), (ii) a round of binding site residue side chain prediction for each of the protein−ligand complexes, (iii) protein minimization of the same set of residues and the ligand for each protein−ligand complex pose, (iv) glide redocking of each protein−ligand complex structure within a specified energy of the lowest-energy structure (30 kcal/mol), and finally (v) estimation of the binding energy (IFDScore) for each result pose. Additional information concerning the target−template alignments, the starting models, and the clustering results is provided as Supporting Information.

RESULTS

Discovery of Novel mOR-EG-Specific Agonists. By coupling mOR-EG activation to the cyclic AMP pathway and the expression of a reporter gene, we screened a large odorant library and discovered 16 novel activating compounds with structures and sizes that significantly differ from 22 previously described ligands (*15*). In addition to eugenol- and vanillin-related compounds, we found three additional classes of mOR-EG-specific agonists comprising benzene derivatives, polycyclic compounds, and cyclohexane derivatives (Figure 1), exhibiting EC_{50} values comparable to that of the primary ligand eugenol. Additional dose−response curves of mOR-EG-specific odorants are shown in the Supporting Information.

With regard to the group of eugenol- and vanillin-related compounds, we observed that methylisoeugenol, which has been described elsewhere as a competitive antagonist of mOR-EG (*42*), behaves as an agonist under our experimental conditions (Figure 1). Our finding has important implications for the mechanism of receptor activation. Whereas Katada et al. (*15*) anticipated that the presence of three substituted groups with a fixed orientation on the benzene ring is a critical structural element of agonists, we found that mOR-EG accepts agonists with a much higher variability in the number and type of substituent on the benzene ring. For instance, the compound Mousse Cristal, a pentasubstituted benzene ring harboring two hydroxyl groups, two methyl groups, and an ester side chain, is a potent agonist similar to eugenol. Dose-dependent activation of mOR-EG was also detected for compounds like raspberry ketone lacking a substituent at position 2 of the phenol ring structure in eugenol (Figure 1).

Furthermore, we discovered that cyclohexane-derived compounds like orivone or *tert*-butylcyclohexanone (TBCHone) were potent agonists (Figure 1), indicating that the aromatic ring found in eugenol and its derivatives is not essential for mOR-EG agonists. This was further supported by our finding that not only monocyclic but also polycyclic ketones like Z95 activate mOR-EG in a dose-dependent fashion, indicating that mOR-EG can bind also significantly larger ligands than previously (*15*) anticipated (Figure 1).

Structural Model of mOR-EG and Docking of Ligands. To probe odorant−receptor interactions at a molecular level, we built a structural model of mOR-EG on the basis of the crystallographic structure of the β2-adrenergic receptor (*26*). The evolutionary relationship and alignment between TM1−4 and TM7 of the β2-adrenergic GPCR and mOR-EG can be readily established. However, because of the low level of sequence homology

Table 1: Effects of Point Mutations on Activation of mOR-EG by Different Odorants[a]

	mutant[b]	ligand	EC_{50} (μM)	EC_{50}(WT)/ EC_{50}(mut)
TM3	C106A	eugenol	41 ± 5	0.3
		MC	59 ± 4	0.4
		Orivone	41 ± 6	0.6
		Wolfwood	no response	0
		MIEG	116 ± 66	0.3
	S113A	eugenol	115 ± 20	0.2
		MC	122 ± 20	0.4
		Orivone	no response	0
		Wolfwood	no response	0
		MIEG	50 ± 10	1.2
	S113T	eugenol	7 ± 2	2.4
		MC	27 ± 21	1.9
		Orivone	39 ± 11	1.5
		Wolfwood	19 ± 3	1.5
		MIEG	47 ± 10	1.3
EL2	F182T	eugenol	no response	0
		MC	104 ± 20	0.2
		Orivone	no response	0
		Wolfwood	no response	0
		MIEG	no response	0
	F182V	eugenol	42 ± 10	0.3
		MC	89 ± 6	0.3
		Orivone	no response	0
		Wolfwood	no response	0
		MIEG	241 ± 339	0.1
TM5	F203W	eugenol	92 ± 7	0.1
		MC	92 ± 18	0.3
		Orivone	no response	0
		Wolfwood	no response	0
		MIEG	no response	0
	N207A	all ligands	no response	0
	E208A	eugenol	52 ± 8	0.2
		MC	54 ± 9	0.5
		Orivone	6 ± 2	0.8
		Wolfwood	7 ± 2	1.3
		MIEG	4 ± 2	6.5
	E208Q	eugenol	48 ± 6	0.2
		MC	77 ± 5	0.3
		Orivone	10 ± 3	2.5
		MIEG	29 ± 8	1
	E208D	eugenol	97 ± 6	0.1
		MC	167 ± 63	0.1
		Orivone	no response	0
		Wolfwood	no response	0
		MIEG	37 ± 4	0.8
	L212V	eugenol	35 ± 13	0.5
		MC	80 ± 11	0.7
		Orivone	97 ± 28	0.6
		Wolfwood	no response	0
		MIEG	118 ± 36	0.5
TM6	F252L	eugenol	60 ± 7	0.3
		MC	137 ± 55	0.4
		Orivone	90 ± 35	0.6
		Wolfwood	no response	0
		MIEG	no response	0
	I256L	eugenol	107 ± 28	0.2
		MC	no response	0
		Orivone	103 ± 28	0.6
		Wolfwood	57 ± 18	0.5
		MIEG	no response	0
	L259V	eugenol	48 ± 10	0.4
		MC	118 ± 24	0.4
		Orivone	no response	0
		Wolfwood	65 ± 17	0.5
		MIEG	124 ± 34	0.5
	Y260F	eugenol	92 ± 8	0.1
		MC	117 ± 3	0.2
		Orivone	no response	0
		Wolfwood	no response	0
		MIEG	no response	0
	Y260L	eugenol	120 ± 22	0.1
		MC	170 ± 47	0.1
		Orivone	no response	0
		Wolfwood	no response	0
		MIEG	no response	0

[a] EC_{50} values of EG, MC, MIEG, OV, and WW obtained from dose−response curves using the SEAP reporter assay measured on wild-type and mutant receptors of mOR-EG as shown in Figure S2 of the Supporting Information. Experiments were performed in triplicate, and data are given as means ± the standard deviation. [b] Amino acids indicated in one-letter code.

between the β2-adrenergic receptor and OR families, the per-residue correspondence in EL2, TM5, and TM6 could not be resolved unambiguously by sequence alignment methods. Therefore, we used a series of alternative alignments to generate an ensemble of comparative receptor models, which were evaluated for consistency with results from mutational analyses, results of Bayesian analysis of mutual information in OR multiple-sequence alignments, and the molecular docking results. In addition, the conformation of EL2 was modeled de novo as described in Materials and Methods. By docking representative agonists of each of the four mOR-EG-specific odorant classes (EG, MIEG, MC, OV, and WW) to the receptor, we identified five amino acids, not investigated previously, that are predicted to be in the proximity of the odorants and therefore to be part of the ligand binding pocket: Cys106 (TM3), Phe182 (EL2), Phe203 (TM5), Glu208 (TM5), and Tyr260 (TM6).

Site-Directed Mutations of Amino Acids. To determine the role of these five residues, they were individually exchanged with other amino acids using site-directed mutagenesis. The thus obtained mutant receptors were analyzed for activation by EG, MIEG, MC, OV, and WW using reporter gene expression as a readout. The same analysis was also performed for point mutations at six other residues (Ser113, Asn207, Leu212, Phe252, Ile256, and Leu259), which were previously shown to be critical for recognition of EG (*15*). The EC_{50} values for activation of the particular mutated mOR-EG are listed in Table 1, and the corresponding dose−response curves are shown in Figure S2 of the Supporting Information. The expression of all mutant receptors on the cell surface was quantified by flow cytometric analysis (Figure S3 of the Supporting Information).

Our structural model of mOR-EG predicts a cluster of polar amino acid residues at the bottom cleft of the binding pocket to be important for ligand recognition. One key residue is Ser113 (TM3), which serves as a hydrogen bond donor for the ligand. The formation of this hydrogen bond was already predicted elsewhere to be essential for eugenol binding (*15*). Our model indicates that Ser113 also plays an important role in binding of other classes of mOR-EG-specific ligands, comprising hydroxyl and keto groups capable of forming hydrogen bonds with Ser113. Accordingly, we found that this residue was sensitive to mutations (summarized in Table 1). The Ser113Ala substitution, for instance, resulted in a complete loss of receptor activation by OV and WW, each possessing only one polar group. For EG, the

EC_{50} was increased ~7-fold. Just for MC, which possesses several polar groups, the EC_{50} increased only ~2-fold, indicating that this ligand favors the hydrogen bonding with Ser113 but is capable of performing alternative polar interactions to activate the receptor (our docking model suggests Asn207, Glu112, and Tyr260 as additional hydrogen bond partners). The Ser113Thr mutant strengthened the hydrophilic interactions with all different classes of ligands as indicated by ~2-fold decreased EC_{50} values (Table 1). This shows that the OH group of the side chain of Ser113 is important for polar interactions with the ligands. The finding that the Ser113Ala substitution does not affect receptor activation by MIEG (Table 1) further suggests that regardless of hydrogen bond formation between a ligand and Ser113 other interactions are effective for achieving receptor activation.

Our docking simulations suggest a hydrophilic cluster of amino acid residues in the binding pocket, comprising Ser113 (TM3), Asn207 (TM5), and Glu208 (TM5). Substitutions of Asn207 abolished the responses to the primary ligand eugenol (*15*). The Asn207Ala mutant also exhibited no detectable activation by EG, MIEG, MC, OV, or WW (Table 1). However, because Asp207Ala is functionally expressed at the cell surface as previously shown (*15*), our results point to a general importance of this residue in ligand recognition. The potential involvement of Asn207 in odorant binding is suggested by our docking results and by the fact that this position is highly variable in the sequence of the OR superfamily (*43*).

Our model predicts Glu208 at a central part of the ligand binding pocket. All substitutions in this position resulted in a significant loss of responsiveness by more polar ligands like EG and MC (Table 1). By contrast, the Glu208Asp and Glu208Ala substitutions yielded slight decreases in the EC_{50} values for more hydrophobic agonists like OV and WW. The Glu208Gln and Glu208Asp substitutions did not significantly alter the responsiveness to MIEG as compared to that of the wild type, but the Glu208Ala substitution strongly decreased the EC_{50} for MIEG ~7-fold (Table 1). Point mutations that replace the negatively charged large side chain of Glu208 with the small uncharged alanine residue seem to create more space at the bottom of the binding pocket, offering a steric advantage for large or lipophilic ligands like WW, OV, or MIEG to interact with Ser113 or Asn207.

Tyr260 is predicted to be located at the membrane−water interface, with the ligand binding pocket pointing its OH group toward the ligand. The Tyr260Phe substitution decreased the EC_{50} values of EG and MC by 5−8-fold and the Tyr260Leu substitution 7−11-fold. Furthermore, the same point mutations completely abolished the responsiveness to OV, WW, and MIEG. Our results indicate that the OH group of Tyr260 is the relevant interacting part of its side chain. However, in addition, hydrophobic interactions with Tyr260 cannot be excluded because the activation by lipophilic ligands (OV, WW, and MIEG) was more affected on mutation than that by ligands having more polar side groups (EG and MC).

Cys106 (TM3) in our model is predicted to be in the vicinity of other functionally important amino acid residues (Asn207 and Glu208). The Cys106Ala substitution slightly affected receptor activation by MC and EG. Their corresponding EC_{50} values increased approximately 3−4-fold, whereas the responsiveness to WW was completely abolished (Table 1). The Cys106Ala substitution had only minor effects on the responsiveness to OV (Table 1). For other mouse ORs, amino acid positions equivalent to mOR-EG's Cys106 were predicted to be involved in odorant recognition (*44*). The results of our point mutation analysis deliver functional evidence of a possible role of Cys106 in ligand binding and discrimination of particular odorant molecules.

Contribution of the Second Extracellular Loop (EL2) to Receptor Activation. Phe182 is located in EL2, which according to the predicted disulfide bond between Cys98 and Cys180 in our structural model projects into the binding pocket and directly interacts with the mOR-EG-specific odorants. It is striking that the Phe182Thr substitution abolished receptor activation by EG, OV, WW, and MIEG and substantially weakened the activity of MC with a 5-fold increase in EC_{50} compared to that of the wild-type receptor (Table1). The Phe182Val substitution showed no activity for OV and WW, a 4−8-fold increase in the EC_{50} for EG and MC, and activation by all the remaining tested odorants. Phe182 corresponds to a presumably conserved odorant interaction site within EL2 (*43*), and our results provide the first functional proof of this prediction.

Contribution of Hydrophobic, Transmembrane Amino Acids to Receptor Activation. Our model predicts an amphipathic ligand binding pocket composed of clusters of hydrophilic amino acids Cys106, Ser113, Asn207, and Tyr260 and a persistent hydrophobic environment. Mutations of amino acids Leu212, Phe252, Ile256, and Leu259 increased the EC_{50} value for EG more than 5-fold and had variable effects on other odorants (Table 1). For instance, the Leu112Val substitution did not alter receptor activation by MC but completely abolished receptor activation by WW. Similarly, a substitution at Phe252 did not have any effects on receptor activation by OV but eliminated the response to WW, supporting the finding of Katada and coworkers (*15*) that these residues are involved in ligand binding; however, they are not equally important for all odorants, as the results of our mutation analysis indicate.

In this study, we also investigated the importance of Phe203, which our model predicted to be located at the periphery of the ligand binding pocket, between TM5 and TM4. This residue might interact with the extended hydrophobic part of larger odorants because this loop region also plays a role in ligand−receptor interactions in the β2-adrenergic receptor. We found that the Phe203Trp substitution in mOR-EG had strong effects on the receptor activation by MC and EG, showing 4−8-fold increased EC_{50} values. The same mutation completely abolished receptor activation by WW and OV, suggesting that Phe203 is involved in ligand−receptor interactions.

DISCUSSION

A restricted set of mOR-EG activating odorants has been reported elsewhere, proposed as a 3-fold substituted benzene ring as the core activating structure (*15*). Here, by random screening of a large odorant library, we found that mOR-EG is activated by a much broader variety of odorant structures. Most strikingly, we discovered that the aromatic, rigid benzene ring is not essential for the activation of mOR-EG. Also, more flexible cyclohexane-based odorants and even polycyclic compounds are potent agonists, indicating that mOR-EG also accepts larger odorants. Furthermore, the receptor tolerates a variety of polar substituents on the benzene ring (hydroxyl, ether, aldehyde, keto, and esterified carboxyl groups) and has no obvious preference for specific structures of apolar side chains. However, in a previous study, it has been pointed out that eugenol derivatives possessing a 1-propenyl group at position 4 of the benzene ring as in the case of methylisoeugenol (MIEG) tend to become mOR-EG-specific antagonists (*42*). The apparent discrepancy between this previous

report and our finding that MIEG is an agonist for mOR-EG might be explained by the observation of another study (*45*) that revealed that distinct odorants act either as agonists or as antagonists depending on the particular G protein presented in the heterologous system. The employment of a nontypical Gα15 in the study of Katada and co-workers (*15*) instead of the natural olfactory $G\alpha_{olf}$ subunit (*46*) as in our study might alter the behavior of mOR-EG toward MIEG, which is an important observation with regard to ligand−OR interactions and the plasticity of OR activation.

Because of the broad structural variations found in the 32 mOR-EG-specific agonists (Figure 1 and ref *15*), it is difficult to define key molecular features of an active ligand. In general, a mOR-EG agonist consists of at least one six-atom, preferentially carbon, ring structure comprising at least one oxygen directly attached to or integrated within the ring. Most agonists carry on the ring an additional hydrophobic substituent, which can be a small unbranched or branched aliphatic group or a larger cyclic hydrocarbon ring. mOR-EG is a receptor accepting a remarkably broad spectrum of agonists. Other ORs have been reported in the literature to be able to bind broad classes of compounds but with different degrees of selectivity. Mouse receptor SR1, for instance, has been identified to respond with stronger intensity to 19 distinct odorants of quite variable structures and functional groups. In contrast to mOR-EG, SR1 does not require cycloalkane or benzene ring structures but accepts linear aliphatic odorants (*17*). In the case of rat ORI7, a wide range of 23 odorants is recognized. ORI7 is highly specific for compounds featuring an aldehyde group but rather unspecific concerning the hydrophobic moiety, which can be a variable-length aliphatic chain or a hexyl ring (*47*). Each of these odorant receptors is obviously capable of binding odorant molecules of a broad range of molecular structures, different sizes, and polar groups. Our molecular models are a first step toward understanding the plasticity of the ligand binding for mOR-EG.

In this study, we have chosen the β2-adrenergic receptor as a homology template for molecular docking studies to predict amino acid residues in mOR-EG critically involved in odorant recognition. The β2-adrenergic receptor belongs to the same class A of the GPCR superfamily as rhodopsin and the ORs. A high-resolution structure is available for the β2-adrenergic receptor (*26*, *35*). The receptor functions like the ORs, as it binds diffusible ligands, whereas bovine rhodopsin has covalently bound its ligand retinal. The β2-adrenergic receptor and ORs exhibit also other common features in the signal transduction mechanism: upon activation they both promote the formation of cyclic adenosine monophosphate (cAMP) via coupling to the adenylate cyclase (*46*, *48*), whereas rhodopsin initiates a different signaling cascade via coupling transducin to phosphodiesterase, which upon activation lowers the intracellular concentration of cyclic guanosine monophosphate (cGMP) (*49*). The extracellular domain is very compact in rhodopsin, shielding the hydrophobic retinal ligand from the aqueous phase, while in the other resolved GPCR structures, the extracellular domain shows a more open conformation to act as a tunnel for diffusible ligands (*26*). How odorants access the binding pocket of its ORs is not known. They might enter the receptor directly from the extramembranous phase. As many odorants are quite hydrophobic, they partition into the hydrophobic cellular membrane, from where they might access the binding pocket in the receptor, as discussed elsewhere for other GPCRs (*50*). Alternatively, odorant binding proteins might function as shuttles for transporting the odorant molecules through the nasal mucus to the hydrophobic ORs and presumably facilitate the uptake of ligands by or their removal from the receptors (*7*, *51*, *52*).

While superimposing our model with the homology model of mOR-EG based on bovine rhodopsin, we found specific differences, which are caused by the choice of the different templates and an alternative target−template alignment. As a consequence, our model of the receptor structure is more open to the extracellular space, shows a different orientation of transmembrane helices TM3 and TM5, and has a different conformation of the second extracellular loop (Figure 2).

The putative odorant binding pocket of our docking of the primary ligand eugenol is to a certain extent in agreement with the model of Katada and co-workers (*15*). It includes several contacts with the bound ligand such as hydrogen bonds at Ser113, hydrophilic interactions with Asn207, and hydrophobic contacts with Leu112, Phe252, Ile256, and Leu259. Here we found additional amino acid contact sites and propose a different orientation for the ligand, which is preferentially parallel to the transmembrane helices and not perpendicular as previously proposed (*15*) (Figure 2). In our model, eugenol occupies a position within the receptor that is closer to the extracellular compartment. Furthermore, the ligand is closer to the critical amino acid residues Phe182, Asn207, and Glu208, and our docking model suggests additional polar contacts with Tyr260, which have not been investigated previously (Figure 2).

After having pointed out these general features of our structural model compared to that of Katada et al. (*15*), we discuss in the following the binding of the four classes of mOR-EG-specific odorants within our model. Particular amino acid residues in predicted transmembrane helices TM3−6 are believed to form the odorant binding pocket of most ORs (*53*, *54*). The binding pocket of mOR-EG according to the predictions of our model is formed by a network of 10 residues distributed on transmembrane helices TM3, TM5, and TM6 toward the extracellular side along with one residue at the second extracellular loop. Via a search for amino acids that are highly conserved in orthologous ORs and less conserved in paralogous ORs, a set of 22 evolutionarily conserved amino acid positions were proposed to form a generalized odorant binding pocket (*43*). Six of these residues (Cys106, Ser113, Phe182, Phe203, Asn207, and Ile256) overlap with our docking model of mOR-EG and were shown in our study to be sensitive to mutations for most of the tested odorants, whereas the model of Katada and co-workers (*15*) shows only four overlaps (Ser113, Phe206, Asn207, and Ile256). In addition, Tyr260 has been suggested to be involved in odorant recognition for other mouse ORs (*44*), for which we delivered the functional proof because mutations of Tyr260 influenced receptor activation by all tested odorants.

The individual docking orientations of EG, MC, OR, and WW are shown in Figure 3. Our analysis suggests that all ligands occupy a similar location within the binding pocket of mOR-EG, including a hydrogen bond with Ser113 that is consistent with our experimental results and the previous docking and mutational study of the binding of eugenol (*15*). The importance of Ser113 for ligand recognition in mOR-EG is underlined by the finding that in human OR1A1 and OR1A2 receptors a corresponding amino acid exists in the form of Ser112, which plays a key role in odorant interaction (*20*). Furthermore, in the rat ORI7 receptor, Cys117 has been shown to be centrally important in odorant recognition, and this position corresponds to Ser113 in mOR-EG (*55*).

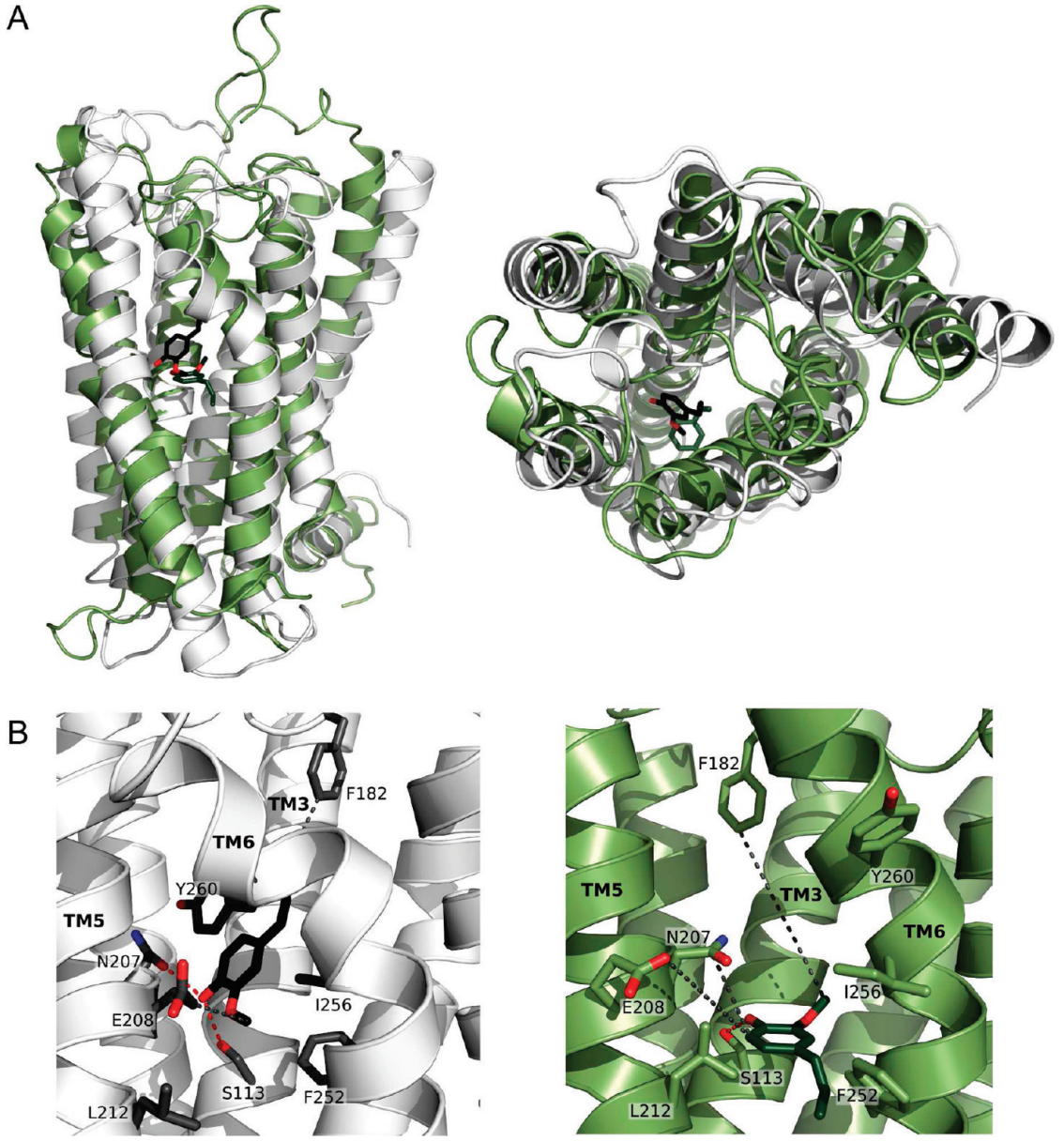

FIGURE 2: Superposition of two homology structural models of mOR-EG with bound eugenol based on the crystal structures of the β2-adrenergic receptor (gray) and rhodopsin (green). (A) Side views with the extracellular side on the top and the intracellular side on the bottom (left) and top views from the extracellular side (right). The backbone structures are represented as ribbons, and the odorant eugenol is represented as sticks [black for our model and dark green for the model of Katada et al. (*15*)]. (B) Interaction of eugenol with amino acid residues in the binding pocket of mOR-EG as found experimentally in our study (left) and that suggested by Katada et al. (*15*) (right). Ser113 forms a hydrogen bond with the OH group of eugenol (red dots) in both models. Potential interactions of eugenol with Asn207 and Glu208 are shown as black dots. In our model, eugenol has a different orientation, occupies an upward shifted position in the receptor, and is closer to amino acid residues Asn207 and Glu208 as in the model of Katada et al. (*15*). Additional amino acid residues lining the binding pocket in our model are Leu212, Phe252, Ile256, and Tyr260. Our predicted three-dimensional structure of the binding pocket of the receptor is in accord with the experimentally determined amino acid contact sites reported in Table 1 and Figure S2 of the Supporting Information.

By probing the potency of our different odorants in activating each of the point mutant ORs, we experimentally identified the residues forming the odorant binding pocket and their relative importance for receptor activation by the different types of agonists as indicated in Figure 3 by color code from white (no effect) to dark red (strong effect).

We also found that mutations of six residues (Ser113, Phe182, Asn207, Phe203, Glu208, and Tyr260) changed receptor activation for all odorants. This is consistent with our model suggesting these residues are part of the ligand binding pocket, with Phe182 located at the second extracellular loop (EL2) at the opening of the ligand binding pocket (Figure 3). Our experimental data show that Phe182 plays an important role in activating mOR-EG by all tested odorants. In our structural model, Cys180 in EL2 forms a disulfide linkage to Cys98 located at the extracellular interface of TM3, and as a consequence, Phe182 in EL2 becomes part of the receptor's ligand binding pocket (Figure 3). There are several observations that support this structural determinant. A corresponding disulfide linkage between EL2 and TM3 was found in many GPCRs, including rhodopsin, adrenergic receptors, adenosine receptors, and angiotensin receptors, to mention a few. Corresponding EL2−TM3 cysteine pairs are also highly conserved in most of the OR sequences (*43*), but EL2 also exhibits structural variations among different GPCRs. It adopts a hairpin structure in bovine rhodopsin (*56*), has an α-helical conformation in β2-adrenergic receptors (*26*), and is unstructured in the

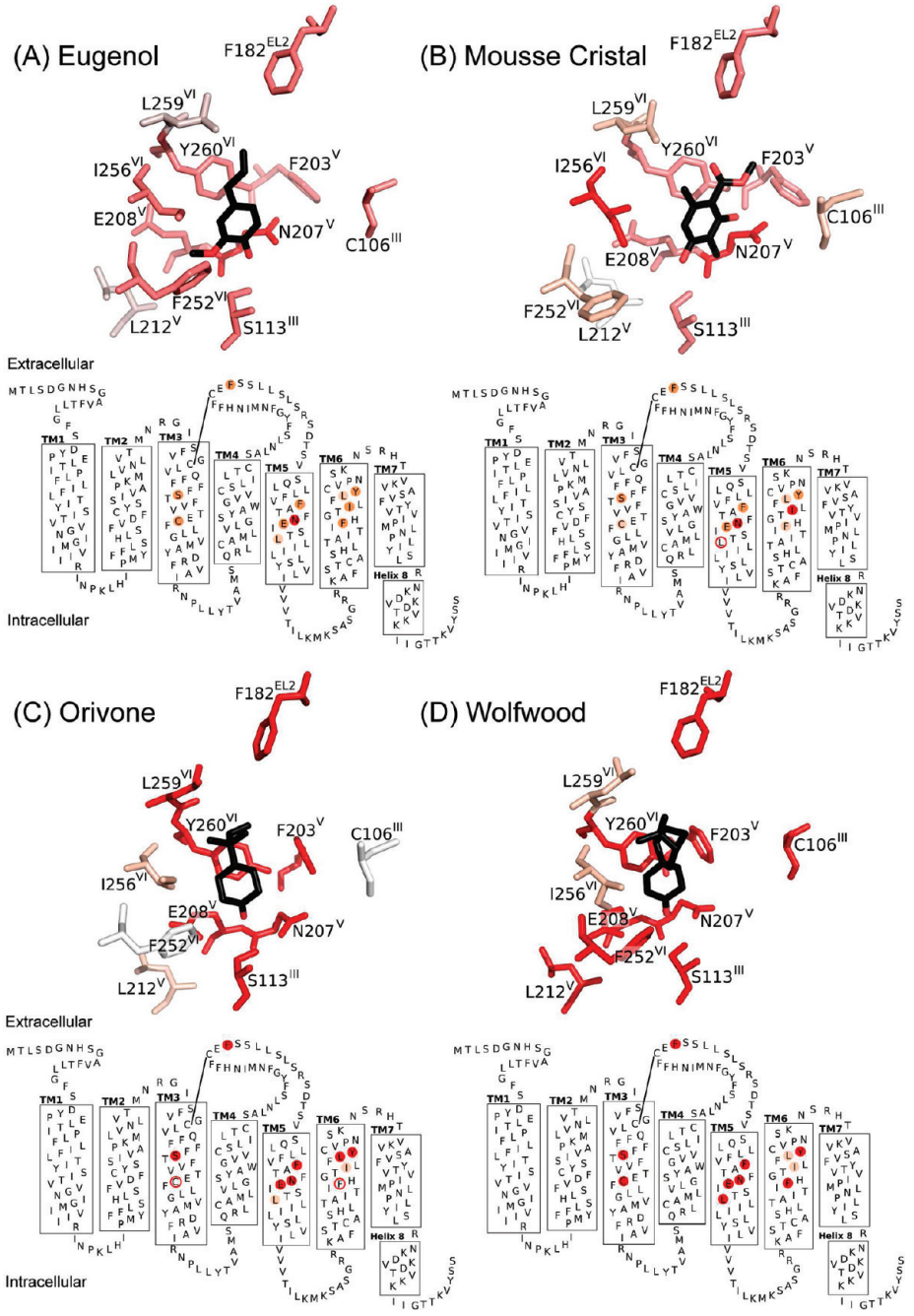

FIGURE 3: Predicted amino acid contact sites of mOR-EG with the odorants eugenol (A), Mousse Cristal (B), Orivone (C), and Wolfwood (D) derived from functional studies of mutant receptor proteins (cf. Table 1 and Figure S2 of the Supporting Information) and shown for each odorant as a snake topology diagram and a three-dimensional (3D) structural model. In the snake diagrams, the OR sequences are represented by the amino acid single-letter code, the transmembrane helices (TM1−7) are depicted as rectangular frames, and mutations of amino acids are highlighted by colored circles. The effects of different point mutations of mOR-EG on the receptor's activation by a particular agonist as reported in Table 1 are represented here by a color code, which is identical in the snake diagrams and in the corresponding 3D docking models. Dark red indicates amino acid point mutations exhibiting strong effects either in loss or in gain of function as compared to wt mOR-EG, more specifically, either yielding no detectable responses to the indicated odorant or significantly decreasing the EC_{50} values compared to that of the wild-type receptor. Red indicates point mutations that cause a strong increase in the EC_{50} values (up to 10-fold). Light red indicates point mutations that cause a modest increase in the EC_{50} values (up to 3-fold). White filled red circles indicate point mutations that did not affect the EC_{50} values. The 3D structural models of the receptor's binding pocket show the orientations of amino acid residues $C106^{III}$, $S113^{III}$, $F182^{EL2}$, $F203^{V}$, $N207^{V}$, $E208^{V}$, $L212^{V}$, $F252^{VI}$, $I256^{VI}$, $L259^{VI}$, and $Y260^{VI}$ (superscripts indicate TM helices in Roman numerals or loop EL2) relative to each of the docked odorants.

A_{2A}-adenosine receptor (*28*). Despite these variations, all known GPCR structures suggest EL2 to take part in ligand binding (*23*, *28*, *56*, *57*). A recent functional study of the angiotensin II type 1 receptor revealed the ability of EL2 to interact with its ligands and to perform agonist-induced conformational changes (*58*). As this report exemplifies how GPCRs generally could bind ligands by EL2, mOR-EG might in analogy interact with odorants in a dynamic manner, influencing the accessibility of the binding cavity for the ligands on their way to and from the binding pocket.

Five amino acids (Cys106, Leu212, Phe252, Ile256, and Leu259) exhibited a variable degree of importance, depending on the specific odorant used in the functional assay. They were sensitive

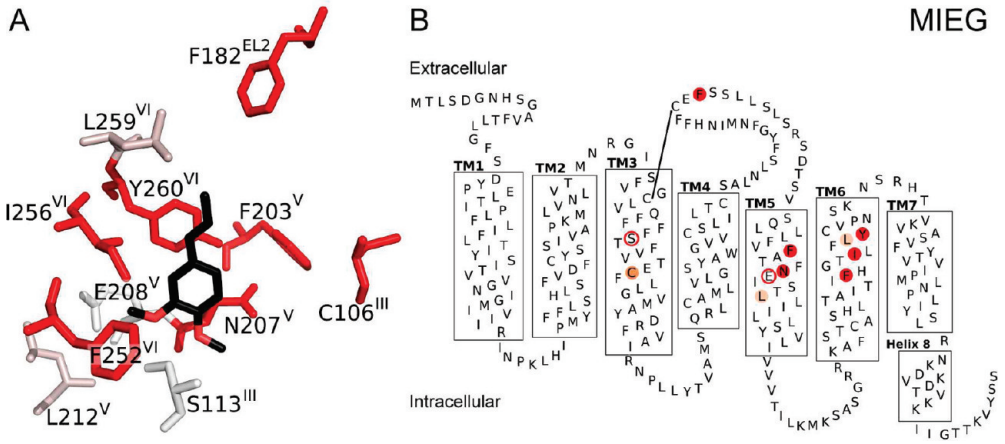

FIGURE 4: Interaction of mOR-EG with MIEG. (A) Close-up of MIEG docked to amino acids $C106^{III}$, $S113^{III}$, $F182^{EL2}$, $F203^{V}$, $N207^{V}$, $E208^{V}$, $L212^{V}$, $F252^{VI}$, $I256^{VI}$, $L259^{VI}$, and $Y260^{VI}$ in the three-dimensional structural model of the receptor's binding pocket (notations as in Figure 3). (B) Snake diagrams of mOR-EG transmembrane topology below docking images. Other notations and color codes as in Figure 3.

to mutations for some of the odorants and less or not sensitive for others (Figure 3), pointing to a higher mobility of these odorants in the binding pocket. This finding suggests that these residues determine the receptor's ligand specificity. The binding of larger odorants like WW is more affected by point mutations, implying that bulkier molecules have more contact sites with the receptor than smaller ligands EG and MC (Figure 3). Also, the less polar odorant OV seems to have a larger number of contact sites with the receptor than MC and EG (Figure 3).

We have also identified MIEG as a mOR-EG-specific agonist. MIEG does not possess polar groups able to form a hydrogen bond with Ser113 like the other ligands (EG, MC, OV, and WW). This could explain why the Ser113Ala substitution has no influence of the receptor's responsiveness to MIEG (Figure 4). Our binding model proposes apolar interactions with amino acid residues Phe182, Phe203, and Tyr260 and polar interactions with Asn207 and Glu208 (Figure 4). Mutations at Tyr260 result in a significant loss of activation of mOR-EG by MIEG (Table 1), which is consistent with our model predicting $\pi-\pi$ interactions between the neighboring aromatic rings of the ligand and the amino acid side chain (Figure 4). The experimental data do not indicate significant polar interactions of MIEG with Glu208. The Glu208Asp and Glu208Gln substitutions reduce the level of activation to an only minor extent, and the Glu208Ala substitution even results in a gain of function, because the EC_{50} significantly decreased compared to that of the wild type (Table 1). The less bulky methyl group of alanine could improve ligand−receptor interactions via additional hydrophobic contacts or reduced steric hindrance in the binding site. The fact that any substitution of Asn207 abolishes receptor activation by MIEG indicates an important role of this residue either directly for ligand binding or more generally in stabilizing the receptor structure. Ligand docking simulations place the propenyl group of MIEG in the proximity of Phe182 in the second extracellular loop. The substitution of Phe182 with valine, exhibiting a less bulky apolar group, generates weak activity, whereas the Phe182Thr mutation completely abolishes activation by MIEG (Table 1). This result indicates that MIEG shares the same orientation in the binding pocket as the other agonists (Figure 4) with hydrophobic contacts around the propenyl substituent. Our results also show that receptor activation does not depend on the interaction of the ligand with Ser113.

In summary, this study delivers detailed information about the ligand binding pocket of a prototypical odorant receptor, mOR-EG. By screening a large odorant compound library, we found a surprisingly wide variety of chemical structures and sizes capable of activating the wild-type receptor. This suggests a high plasticity of the receptor's binding pocket and perhaps a high mobility of the ligands within the pocket, which could explain why the dose−response curves for receptor activation are spread over 3 orders of magnitude of agonist concentration. From the activation profiles of mutant receptors with single-amino acid replacements located around a predicted receptor ligand binding region, we finally localized in the receptor protein sequence 11 amino acid residues contacting a bound agonist odorant molecule. Thereby, we precisely defined the amino acid composition of the ligand binding pocket of mOR-EG. Using homology modeling, we finally predicted the three-dimensional structure with the docked ligand for each case of the receptor activating odorant. Unraveling key amino acid residues involved in odorant−receptor interactions also might be important for designing novel synthetic ligands (*59*). Because of the lack of high-resolution OR structures, docking of odorants to OR structure models must be considered with caution. However, the close agreement between our functional mutagenesis studies and our docking results delivers confidence in the molecular details we have obtained for the ligand binding pocket of mOR-EG. Our discovery of receptor-specific functional fingerprints of receptor−ligand interactions might be of functional importance for olfaction.

The existence of a class of broadly tuned low-affinity ORs has been hypothesized to exist and to function as odor intensity detectors (*60*). In this study, we have discovered that mOR-EG is activated by a large number of odorants at concentrations similar to the concentrations required to activate more selective receptors in similar functional assays (*61*). Therefore, we conclude that mOR-EG might encode odorant character rather than odor intensity. This finding also has implications for olfactory processing, because our results provide evidence that already at the level of a distinct OR dense odorant information is perceived to be transmitted to the brain. This is consistent with functional analyses in the olfactory bulb that apart from sparse glomerular inputs (*62*) glomeruli with a large diversity of chemical spectra also can be observed (*63*).

Our understanding of the mechanisms of odor perception is still in its infancy. Novel approaches are required for unravelling the molecular basis of olfaction, for example, by extending the functional studies to larger OR libraries (*61*) if possible in

primary olfactory cells where activation of properly labeled ORs might be followed on a molecular level by optical imaging (*10*, *64*). On the other hand, high-resolution structures of ORs are desperately required, and the recent isolation of large quantities of odorant receptors for structural and biophysical studies is a first step in this direction (*11*).

ACKNOWLEDGMENT

We thank Sayako Katada and Kazushige Touhara for kindly providing their model of the mouse eugenol receptor based on the rhodopsin template and for a set of point mutations introduced into mOR-EG cDNA. We are grateful to Luigino Grasso for his assistance in flow cytometry analysis and to Joachim Piguet for his support in informatics. Financial support from SystemsX program is acknowledged.

SUPPORTING INFORMATION AVAILABLE

Supplemental dose−response curves of mOR-EG-specific odorants (Figure S1), effects of mOR-EG point mutations on odorant dose−response curves (Figure S2), flow cytometry analysis of the cell surface expression of wild-type and mutant mOR-EGs (Figure S3), multiple-amino acid sequence alignments between the human β2 adrenergic receptor and mouse mOR-EG (Figure S4), superpositions of the favored mOR-EG model and models generated by alternative alignments (Figure S5), most populated clusters of conformations for the second extracellular loop, EL2 (Figure S6), and agreement of models generated by alternative alignments with GPCR fingerprints and Bayesian pairwise residue interactions and mutational data (Table S1). This material is available free of charge via the Internet at http://pubs.acs.org.

REFERENCES

1. Buck, L., and Axel, R. (1991) A novel multigene family may encode odorant receptors: A molecular basis for odor recognition. *Cell 65*, 175–187.
2. Zozulya, S., Echeverri, F., and Nguyen, T. (2001) The human olfactory receptor repertoire. *Genome Biol. 2*, 0018.0011–0018.0012.
3. Malnic, B., Godfrey, P. A., and Buck, L. B. (2004) The human olfactory receptor gene family. *Proc. Natl. Acad. Sci. U.S.A. 101*, 2584–2589.
4. Godfrey, P. A., Malnic, B., and Buck, L. B. (2004) The mouse olfactory gene family. *Proc. Natl. Acad. Sci. U.S.A. 101*, 2156–2161.
5. Mombaerts, P. (2006) Axonal wiring in the mouse olfactory system. *Annu. Rev. Cell Dev. Biol. 22*, 713–737.
6. Breer, H. (2008) The sense of smell: Reception of flavors. *Ann. N.Y. Acad. Sci. 1126*, 1–6.
7. Breer, H. (2003) Olfactory receptors: Molecular basis for recognition and discrimination of odors. *Anal. Bioanal. Chem. 377*, 427–433.
8. Murrell, J. R., and Hunter, D. D. (1999) An olfactory sensory neuron line, odora, properly targets olfactory proteins and reponds to odorants. *J. Neurosci. 19*, 8260–8270.
9. Zhuang, H., and Matsunami, H. (2008) Evaluating cell-surface expression and measuring activation of mammalian odorant receptors in heterologous cells. *Nat. Protoc. 3*, 1402–1413.
10. Jacquier, V., Prummer, M., Segura, J. M., Pick, H., and Vogel, H. (2006) Visualizing odorant receptor trafficking in living cells down to the single-molecule level. *Proc. Natl. Acad. Sci. U.S.A. 103*, 14325–14330.
11. Cook, B. L., Steuerwald, D., Kaiser, L., Graveland-Bikker, J., Vanberghem, M., Berke, A. P., Herlihy, K., Pick, H., Vogel, H., and Zhang, S. (2009) Large-scale production and study of a synthetic G protein-coupled receptor: Human olfactory receptor 17-4. *Proc. Natl. Acad. Sci. U.S.A. 106*, 11925–11930.
12. Malnic, B., Hirono, J., Sato, T., and Buck, L. B. (1999) Combinatorial receptor codes for odors. *Cell 96*, 713–723.
13. Krautwurst, D., Yau, K. W., and Reed, R. R. (1998) Identification of ligands for olfactory receptors by functional expression of a receptor library. *Cell 95*, 917–926.
14. Bozza, T., Feinstein, P., Zheng, C., and Mombaerts, P. (2002) Odorant receptor expression defines functional units in the mouse olfactory system. *J. Neurosci. 22*, 3033–3043.
15. Katada, S., Hirokawa, T., Oka, Y., Suwa, M., and Touhara, K. (2005) Structural basis for a broad but selective ligand spectrum of a mouse olfactory receptor: Mapping the odorant-binding site. *J. Neurosci. 25*, 1806–1815.
16. Jacquier, V., Pick, H., and Vogel, H. (2006) Characterization of an extended receptive ligand repertoire of the human olfactory receptor OR17-40 comprising structurally related compounds. *J. Neurochem. 97*, 537–544.
17. Grosmaitre, X., Fuss, S. H., Lee, A. C., Adipietro, K. A., Matsunami, H., Mombaerts, P., and Ma, M. (2009) SR1, a mouse odorant receptor with an unusually broad response profile. *J. Neurosci. 29*, 14545–14552.
18. Abaffy, T., Malhotra, A., and Luetje, C. W. (2007) The molecular basis for ligand specificity in a mouse olfactory receptor: A network of functionally important residues. *J. Biol. Chem. 282*, 1216–1224.
19. Kato, A., and Touhara, K. (2009) Mammalian olfactory receptors: Pharmacology, G protein coupling and desensitization. *Cell. Mol. Life Sci. 66*, 3743–3753.
20. Schmiedeberg, K., Shirokova, E., Weber, H. P., Schilling, B., Meyerhof, W., and Krautwurst, D. (2007) Structural determinants of odorant recognition by the human olfactory receptors OR1A1 and OR1A2. *J. Stuct. Biol. 159*, 400–412.
21. Pick, H., Etter, S., Baud, O., Schmauder, R., Bordoli, L., Schwede, T., and Vogel, H. (2009) Dual activities of odorants on olfactory and nuclear hormone receptors. *J. Biol. Chem. 284*, 30547–30555.
22. Lundström, K. (2005) The future of G protein-coupled receptors as targets in drug discovery. *IDrugs 8*, 909–913.
23. Palczewski, K., Kumasaka, T., Hori, T., Behnke, C. A., Motoshima, H., Fox, B. A., Le Trong, I., Teller, D. C., Okada, T., Stenkamp, R. E., Yamamoto, M., and Miyano, M. (2000) Crystal structure of rhodopsin: A G protein-coupled receptor. *Science 289*, 739–745.
24. Scheerer, P., Park, J. H., Hildebrand, P. W., Kim, Y. J., Krauss, N., Choe, H. W., Hofmann, K. P., and Ernst, O. P. (2008) Crystal structure of opsin in its G-protein-interacting conformation. *Nature 455*, 497–502.
25. Park, J. H., Scheerer, P., Hofmann, K. P., Choe, H. W., and Ernst, O. P. (2008) Crystal structure of the ligand-free G-protein-coupled receptor opsin. *Nature 454*, 183–187.
26. Rasmussen, S. G., Choi, H. J., Rosenbaum, D. M., Kobilka, T. S., Thian, F. S., Edwards, P. C., Burghammer, M., Ratnala, V. R., Sanishvili, R., Fischetti, R. F., Schertler, G. F., Weis, W. I., and Kobilka, B. K. (2007) Crystal structure of the human β2 adrenergic G-protein-coupled receptor. *Nature 450*, 383–387.
27. Warne, T., Serrano-Vega, M. J., Baker, J. G., Moukhametzianov, R., Edwards, P. C., Henderson, R., Leslie, A. G., Tate, C. G., and Schertler, G. F. (2008) Structure of a β1-adrenergic G-protein-coupled receptor. *Nature 454*, 486–491.
28. Jaakola, V. P., Griffith, M. T., Hanson, M. A., Cherezov, V., Chien, E. Y., Lane, J. R., Ijzerman, A. P., and Stevens, R. C. (2008) The 2.6 Å crystal structure of a human A2A adenosine receptor bound to an antagonist. *Science 322*, 1211–1217.
29. Wu, B., Chien, E. Y., Mol, C. D., Fenalti, G., Liu, W., Katritch, V., Abagyan, R., Brooun, A., Wells, P., Bi, F. C., Hamel, D. J., Kuhn, P., Handel, T. M., Cherezov, V., and Stevens, R. C. (2010) Structures of the CXCR4 chemokine GPCR with small-molecule and cyclic peptide antagonists. *Science 330*, 1066–1071.
30. Chien, E. Y. T., Liu, W., Zhao, Q., Katritch, V., Won Han, G., Hanson, M. A., Shi, L., Hauck Newman, A., Javitch, J. A., Cherezov, V., and Stevens, R. C. (2010) Structure of the human dopamine D3 receptor in complex with a D2/D3 selective antagonist. *Science 330*, 1091–1095.
31. Hofmann, K. P., Scheerer, P., Hildebrand, P. W., Choe, H. W., Park, J. H., Heck, M., and Ernst, O. P. (2009) A G protein-coupled receptor at work, the rhodopsin model. *Trends Biochem. Sci. 34*, 540–552.
32. Worth, C. L., Kleinau, G., and Krause, G. (2009) Comparative sequence and structural analyses of G-protein-coupled receptor crystal structures and implications for molecular models. *PLoS One 4*, e7011.
33. Floriano, W. B., Vaidehi, N., Goddard, W. A., III, Singer, M. S., and Shepherd, G. M. (2000) Molecular mechanisms underlying differential odor responses of a mouse olfactory receptor. *Proc. Natl. Acad. Sci. U.S.A. 97*, 10712–10716.
34. Saito, H., Kubota, M., Roberts, R. W., Chi, Q., and Matsunami, H. (2004) RTP family members induce functional expression of mammalian odorant receptors. *Cell 119*, 679–691.
35. Cherezov, V., Rosenbaum, D. M., Hanson, M. A., Rasmussen, S. G., Thian, F. S., Kobilka, T. S., Choi, H. J., Kuhn, P., Weis, W. I.,

Kobilka, B. K., and Sevens, R. C. (2007) High-resolution crystal structure of an engineered human β2-adrenergic G protein-coupled receptor. *Science 318*, 1258–1265.
36. Armougom, F., Moretti, S., Poirot, O., Audic, S., Dumas, P., Schaeli, B., Keduas, V., and Notredame, C. (2006) Expresso: Automatic incorporation of structural information in multiple sequence alignments using 3D-Coffee. *Nucleic Acids Res. 34*, W604–W608.
37. Burger, L., and van Nimwegen, E. (2008) Accurate prediction of protein-protein interactions from sequence alignments using a Bayesian method. *Mol. Syst. Biol. 4*, 165.
38. Bissantz, C., Logean, A., and Rognan, D. (2004) High-throughput modeling of human G-protein coupled receptors: Amino acid sequence alignment, three-dimensional model building, and receptor library screening. *J. Chem. Inf. Comput. Sci. 44*, 1162–1176.
39. Sali, A., and Blundell, T. L. (1993) Comparative protein modelling by satisfaction of spatial restrains. *J. Mol. Biol. 234*, 779–815.
40. Wang, C., Bradley, P., and Baker, D. (2007) Protein-protein docking with backbone flexibility. *J. Mol. Biol. 373*, 503–519.
41. Sherman, W., Day, T., Jacobson, M. P., Friesner, R. A., and Farid, R. (2006) Novel procedure for modeling ligand/receptor induced fit effects. *J. Med. Chem. 49*, 534–553.
42. Oka, Y., Omura, M., Kataoka, H., and Touhara, K. (2004) Olfactory receptor antagonism between odorants. *EMBO J. 23*, 120–126.
43. Man, O., Gilad, Y., and Lancet, D. (2004) Prediction of the odorant binding site of olfactory receptor proteins by human-mouse comparisons. *Protein Sci. 13*, 240–254.
44. Khafizov, K., Anselmi, C., Menini, A., and Carloni, P. (2007) Ligand specificity of odorant receptors. *J. Mol. Model. 13*, 401–409.
45. Shirokova, E., Schmiedeberg, K., Bedner, P., Niessen, H., Willecke, K., Raguse, J. D., Meyerhof, W., and Krautwurst, D. (2005) Identification of specific ligands for orphan olfactory receptors. G protein-dependent agonism and antagonism of odorants. *J. Biol. Chem. 280*, 11807–11815.
46. Kaupp, U. B. (2010) Olfactory signaling in vertebrates and insects: Differences and commonalities. *Nat. Rev. Neurosci. 11*, 188–200.
47. Araneda, R. C., Kini, A. D., and Firestein, S. (2000) The molecular receptive range of an odorant receptor. *Nat. Neurosci. 3*, 1248–1255.
48. Ostrom, R. S., Liu, X., Head, B. P., Gregorian, C., Seasholtz, T. M., and Insel, P. A. (2002) Localization of adenylate cyclase isoforms and G protein-coupled receptors in vascular smooth musle cells: Expression in caveolin-rich and noncaveolin domains. *Mol. Pharmacol. 62*, 983–992.
49. Goc, A., Angel, T. E., Jastrzebska, B., Wang, B., Wintrode, P. L., and Palczewski, K. (2008) Different properties of the native and reconstituted heteromeric G protein transducin. *Biochemistry 47*, 12409–12419.
50. Sargent, D. F., and Schwyzer, R. (1986) Membrane lipid phase as a catalyst for peptide-receptor interactions. *Proc. Natl. Acad. Sci. U.S.A. 83*, 5774–5778.
51. Borysik, A. J., Briand, L., Taylor, A. J., and Scott, D. J. (2010) Rapid odorant release in mammalian odour binding proteins facilitates their temporal coupling to odorant signals. *J. Mol. Biol. 404*, 372–380.
52. Taylor, A. J., Cook, D. J., and Scott, D. J. (2008) Role of odorant binding proteins: Comparing hypothetical mechanisms with experimental data. *Chem. Percept. 1*, 153–162.
53. Menini, A., Lagostena, L., and Boccaccio, A. (2004) Olfaction: From odorant molecules to the olfactory cortex. *News Physiol. Sci. 19*, 101–104.
54. Floriano, W. B., Vaidehi, N., and Goddard, W. A., III (2004) Making sense of olfaction through predictions of the 3-D structure and function of olfactory receptors. *Chem. Senses 29*, 269–290.
55. Hall, S. E., Floriano, W. B., Vaidehi, N., and Goddard, W. A., III (2004) Predicted 3-D structures for mouse I7 and rat I7 olfactory receptors and comparison of predicted odor recognition profiles with experiment. *Chem. Senses 29*, 595–616.
56. Park, J. H., Scheerer, P., Hofmann, K. P., Choe, H. W., and Ernst, O. P. (2008) Crystal structure of opsin in its G-protein-interacting conformation. *Nature 454*, 183–187.
57. Singer, M. S., Oliveira, L., Vriend, G., and Shepherd, G. M. (1995) Potential ligand-binding residues in rat olfactory receptors identified by correlated mutation analysis. *Recept. Channels 3*, 89–95.
58. Unal, H., Jagannathan, R., Bhat, M. B., and Karnik, S. S. (2010) Ligand-specific conformation of extracellular loop-2 in the angiotensin II type 1 receptor. *J. Biol. Chem. 285*, 16341–16350.
59. Doszczak, L., Kraft, P., Weber, H. P., Bertermann, R., Triller, A., Hatt, H., and Tacke, R. (2007) Prediction of perception: Probing the hOR17-4 olfactory receptor model with silicon analogues of bourgeonal and lilial. *Angew. Chem., Int. Ed. 46*, 3367–3371.
60. Firestein, S. (2001) How the olfactory system makes sense of scent. *Nature 413*, 211–218.
61. Saito, H., Chi, Q., Zhuang, H., Matsunami, H., and Mainland, J. D. (2009) Odor coding by a mammalian receptor repertoire. *Sci. Signaling 2*, ra9.
62. Fantana, A. L., Soucy, E. R., and Meister, M. (2008) Rat olfactory bulb mitral cells receive sparse glomerular inputs. *Neuron 59*, 802–814.
63. Soucy, E. R., Albeanu, D. F., Fantana, A. L., Murthy, V. N., and Meister, M. (2008) Precision and diversity in an odor map on the olfactory bulb. *Nat. Neurosci. 12*, 210–220.
64. Meyer, B. H., Segura, J. M., Martinez, K. L., Hovius, R., George, N., Johnsson, K., and Vogel, H. (2006) FRET imaging reveals that functional neurokinin-1 receptors are monomeric and reside in membrane microdomains of live cells. *Proc. Natl. Acad. Sci. U.S.A. 103*, 2138–2143.